A Time-Split Discontinuous Galerkin Global Nonhydrostatic Dynamical Core

Ram D. Nair

Michael Toy
Computational Information Systems Laboratory
National Center for Atmospheric Research, Boulder, CO, USA

Lei Bao
University of Colorado, Boulder, CO, USA

[Galerkin methods with applications in weather and climate forecasting,
March 23rd–27th, 2015, ICMS, Edinburgh]

Overview

- Motivation
- Non-Hydrostatic HOMME
    1. Basic Design (HOMAM)
    2. Compressible Euler system for Cubed-Sphere
    3. Vertical Terrain-following Coordinates
    4. DG Discretization
- Diffusion Process with LDG/FR approaches
- Time Stepping Methods (HEVI)
- HOMAM: 3D Advection Tests
    1. DCMIP Benchmark Results
    2. Monotonic Limiting & Positivity Preservation
- Nonhydrostatic (NH) Test Results
    1. HEVI convergence 2D Case
    2. 3D NH Gravity Wave tests
    3. Comparison of LDG/FR diffusion with Straka Test
    4. Performance of HEVI with Schär Mountain test
- Summary

Non-Hydrostatic HOMME: Why do we need this?

- The High-Order Method Modeling Environment (HOMME) is a petascale capable hydrostatic dynamical core developed at NCAR and DOE labs. HOMME/SE version is currently used for climate simulation.
- Hydrostatic dynamics is not suitable or valid for horizontal resolution less than 10 KM ($1/8°$)
- Simulate atmospheric dynamics at ultra high-resolution (global cloud-system resolving model)
- Toward exa-scale computing, more accurate climate simulation
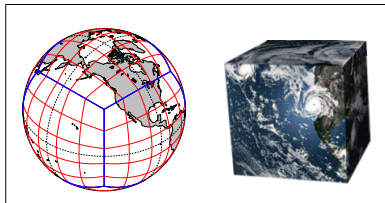
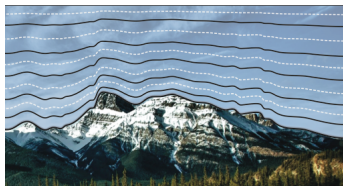Two modeling efforts are under development

- Direct extension of HOMME SE (or CAM-SE) hydrostatic model to a non-hydrostatic model (ACME: D. Hall & M. Taylor + ...)
- Solve the classical fully compressible 3D Euler system on the cubed-sphere using DG Method
- The DG/NH model development in HOMME framework at NCAR is named as the High-Order Multiscale Atmospheric Model ("HOMAM")

HOMAM Development in HOMME Framework

- Horizontal Grid system (Cubed-Sphere)

- HOMME hydrostatic framework is based on cubed-sphere geometry (Sadourny, 1972). Sepctral Element (SE) and discontinuous Galerkin (DG) methods are used for spatial discretization
- Quasi-uniform rectangular mesh, well suited for the element-based methods such as DG or SE methods.
- Proven petascale capability (Dennis et al. 2012). Horizontal design (MPI/parallel) is adopted for the new model.

- Vertical Grid system (z-coordinate)

- HOMME currently employs pressure-based η-coordinates in the vertical with FD discretization
- Replace by the terrain-following height-based vertical z coordinates. Dimension splitting (2D + 1D) spatial discretization with DG methods.

Non-Hydrostatic (NH) Model Development: Basic Design

- Atmosphere: 3D Spherical domain (shell) with the vertical (radial direction) length scale $\mathscr{O}(10)$ km and the horizontal length scale $\mathscr{O}(10,000)$ km.

- The dynamics is governed by 3D compressible Euler/Navier-Stokes system of equations, based on conservation of mass, energy, momentum etc.

$$\frac{\partial \rho}{\partial t} + \nabla \cdot (\rho \mathbf{V}) = 0$$

$$\frac{\partial \rho \mathbf{V}}{\partial t} + \nabla \cdot (\rho \mathbf{V} \otimes \mathbf{V}) = -\nabla p' - (\rho - \overline{\rho})g\mathbf{k} - 2\rho \Omega \times \mathbf{V} + \mathbf{F}_M$$

$$\frac{\partial \rho \theta}{\partial t} + \nabla \cdot (\rho \theta \mathbf{V}) = 0$$

$$\frac{\partial \rho q_k}{\partial t} + \nabla \cdot (\rho q_k \mathbf{V}) = 0$$

$\mathbf{V} = (u,v,w)$ 3D wind field, ρ air density, p pressure, θ potential temperature, q_k moisture variables, Ω erath's rotation rate, $\mathbf{F}_M$ diffusive fluxes and forcring etc.

Compressible Euler System in Generalized Coordinates

- The 3D compressible Euler system of equations on a rotating sphere in generalized curvilinear coordinates (x^1, x^2, x^3) can be written in tensor form (*Warsi, 1992*):

$$\frac{\partial \rho}{\partial t} + \frac{1}{\sqrt{G}} \left[\frac{\partial}{\partial x^j} (\sqrt{G} \rho u^j) \right] = 0 \quad \{\text{Summation Implied}\}$$

$$\frac{\partial \rho u^i}{\partial t} + \frac{1}{\sqrt{G}} \left[\frac{\partial}{\partial x^j} [\sqrt{G} (\rho u^i u^j + p G^{ij})] \right] + \Gamma^i_{jk} (\rho u^j u^k + p G^{jk}) = f \sqrt{G} (u^1 G^{2i} - u^2 G^{1i}) - \rho g G^{3i}$$

$$\frac{\partial \rho \theta}{\partial t} + \frac{1}{\sqrt{G}} \left[\frac{\partial}{\partial x^j} (\sqrt{G} \rho \theta u^j) \right] = 0$$

$$\frac{\partial \rho q}{\partial t} + \frac{1}{\sqrt{G}} \left[\frac{\partial}{\partial x^j} (\sqrt{G} \rho q u^j) \right] = 0$$

- Where u^i is contravariant wind field, G_{ij} metric tensor, $\sqrt{G} = |G_{ij}|^{1/2}$ is the Jacobian of the transform, $G^{ij} = (G_{ij})^{-1}$, and $i, j, k \in \{1, 2, 3\}$. The associated Christoffel symbols (second kind) are defined as

$$\Gamma^i_{jk} = \frac{1}{2} G^{il} \left[\frac{\partial G_{kl}}{\partial x^j} + \frac{\partial G_{jl}}{\partial x^k} - \frac{\partial G_{kj}}{\partial x^l} \right]$$

- Mathematically elegant but computationally cumbersome!

## Model Equations for the Cubed-Sphere Geometry
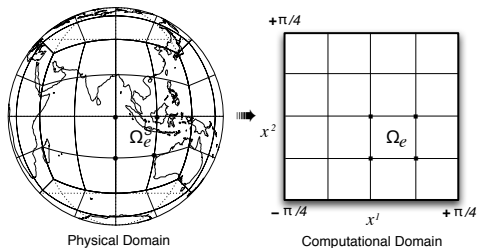
- Equiangular central projection
- Curvilinear horizontal coordinates (x^1, x^2)
- 6 patched domains, $x^1, x^2 \in [-\pi/4, \pi/4]$
- "Cartesian-like" computational domains

Physical Domain   Computational Domain

- Shallow (thin) atmosphere approximation makes the the spherical domain as a vertically stacked cubed-sphere layers.
- $x^3 =$ radius $r+$ height z, s.t $z \ll r \implies (x^1, x^2, x^3) \to (x^1, x^2, z)$
- The metric tensor associated with shallow atmosphere takes a simple form,

$$
G_{ij} = \begin{bmatrix} \hat{G}_{11} & \hat{G}_{12} & 0 \\ \hat{G}_{21} & \hat{G}_{22} & 0 \\ 0 & 0 & 1 \end{bmatrix}, \quad \hat{G}_{ij} = \frac{r^2}{\mu^4 \cos^2 x^1 \cos^2 x^2} \begin{bmatrix} 1 + \tan^2 x^1 & -\tan x^1 \tan x^2 \\ -\tan x^1 \tan x^2 & 1 + \tan^2 x^2 \end{bmatrix},
$$

where $i, j \in \{1, 2\}$ and $\mu^2 = 1 + \tan^2 x^1 + \tan^2 x^2$. Jacobian $\sqrt{G_h} \equiv |G_{ij}|^{1/2} = |\hat{G}_{ij}|^{1/2}$

HOMAM: Vertical Grid System
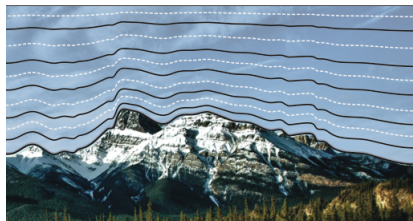
- Terrain-following height-based vertical z coordinate.
- Multiple options [e.g., Schär (2002), Klemp (2011), SLEVE]
- Vertical coordinate transformation (Gal-Chen & Somerville, JCP 1975), is currently adopted.

- $h_s = h_s(x^1, x^2)$ is the prescribed mountain profile and z_{top} is the top of the model domain

$$\zeta = z_{top} \frac{z - h_s}{z_{top} - h_s}, \quad z(\zeta) = h_s(x^1, x^2) + \zeta \frac{z_{top} - h_s}{z_{top}}; \quad h_s \leq z \leq z_{top}.$$

- The Jacobian associated with the transform $(x^1, x^2, z) \rightarrow (x^1, x^2, \zeta)$ is

$$\sqrt{G_v} = \left[\frac{\partial z}{\partial \zeta} \right]_{(x^1, x^2)} = 1 - \frac{h_s(x^1, x^2)}{z_{top}}$$

HOMAM: Vertical Coordinate Transform, $(x^1, x^2, z) \rightarrow (x^1, x^2, \zeta)$

- The vertical 'physical' velocity $w = dz/dt$, in (x^1, x^2, z) system
- Vertical velocity in the transformed (x^1, x^2, ζ) system is $u^3 = \tilde{w}$,

$$\tilde{w} = \frac{d\zeta}{dt}, \quad \sqrt{G_v}\tilde{w} = w + \sqrt{G_v}G_v^{13}u^1 + \sqrt{G_v}G_v^{23}u^2,$$

  where (u^1, u^2) contravariant wind vectors on the cubed-sphere surface.

- Metric coefficients (*Clark 1977, JCP*)

$$\sqrt{G_v} = \left[\frac{\partial z}{\partial \zeta}\right]_{(x^1, x^2)}, \quad \sqrt{G_v}G_v^{13} \equiv \left[\frac{\partial h_s}{\partial x^1}\right]_{(z)}\left(\frac{\zeta}{z_{top}} - 1\right), \quad \sqrt{G_v}G_v^{23} \equiv \left[\frac{\partial h_s}{\partial x^2}\right]_{(z)}\left(\frac{\zeta}{z_{top}} - 1\right).$$

- Treating $\tilde{w}$ as a prognostic variable in the vertical momentum equations results in several Christoffel symbols Γ_{jk}^i in the source term — computationally undesirable!

- Remedy: Treat w as the prognostic variable [*Vinokur (1974), Clark (1977), Satoh (2003)*]. To preserve the flux-form, use the following differential transforms:

- The spacial derivates for an arbitrary scalar ψ can be written in terms of the transformed vertical ζ-coordinate as follows:

$$\sqrt{G_v}\frac{\partial \psi}{\partial z} = \frac{\partial \psi}{\partial \zeta}, \quad \sqrt{G_v}\frac{\partial \psi}{\partial x^i} = \frac{\partial(\sqrt{G_v}\psi)}{\partial x^i} + \frac{\partial(\sqrt{G_v}G_v^{i3}\psi)}{\partial \zeta}, \quad i = 1, 2.$$

HOMAM: Vertical Coordinate Transform

- Simplifications lead to logically "Cartesian-like" model equations.
- Vertical momentum equation in the familiar (x, y, z) coordinate

$$\frac{\partial(\rho w)}{\partial t} + \frac{\partial(\rho w u)}{\partial x} + \frac{\partial(\rho w v)}{\partial y} + \frac{\partial[\rho w w + p']}{\partial z} = -\rho' g$$

- The w-Eqn in (x^1, x^2, ζ) system takes the following form:

$$\frac{\partial(\sqrt{G}\rho w)}{\partial t} + \frac{\partial(\sqrt{G}\rho w u^1)}{\partial x^1} + \frac{\partial(\sqrt{G}\rho w u^2)}{\partial x^2} + \frac{\partial[\sqrt{G}\rho w \tilde{w} + \sqrt{G_h}\, p']}{\partial \zeta} = -\sqrt{G}\rho' g,$$

where $\sqrt{G} = \sqrt{G_h}\sqrt{G_v}$, the product of horizontal and vertical time-independent Jacobins.

- The Euler system in (x^1, x^2, ζ) coordinates can be written in the following compact (flux) form,

$$\frac{\partial \mathbf{U}}{\partial t} + \frac{\partial \mathbf{F}_1}{\partial x^1} + \frac{\partial \mathbf{F}_2}{\partial x^2} + \frac{\partial \mathbf{F}_3}{\partial \zeta} = \mathbf{S}(\mathbf{U})$$

where $\mathbf{U}$ is the state vector and $\mathbf{F}_1, \mathbf{F}_2, \mathbf{F}_3$ are the flux functions along the coordinate direction, and $\mathbf{S}(\mathbf{U})$ denote the source vector.

- Decompose ρ, θ and p as the sum of a mean-state $\overline{(.)}$ and perturbation $(.)'$ such that $\rho = \overline{\rho} + \rho'$, $\theta = \overline{\theta} + \theta'$, $p = \overline{p} + p'$, $(\rho\theta) = \overline{\rho\theta} + (\rho\theta)'$.
- The mean-state maintains hydrostatic balance $\frac{d\overline{p}}{dz} = -\overline{\rho} g$.

HOMAM: Governing Equations in (x^1, x^2, ζ) system

- Final form of the 'perturbed' Euler system in (x^1, x^2, ζ) 3D Cubed-sphere

$$\frac{\partial \mathbf{U}}{\partial t} + \frac{\partial \mathbf{F}_1}{\partial x^1} + \frac{\partial \mathbf{F}_2}{\partial x^2} + \frac{\partial \mathbf{F}_3}{\partial \zeta} = \mathbf{S}(\mathbf{U}) \Rightarrow \quad \frac{\partial \mathbf{U}}{\partial t} + \nabla \cdot \mathbf{F}(\mathbf{U}) = \mathbf{S}(\mathbf{U})$$

$$\mathbf{U} = \begin{bmatrix} \sqrt{G}\rho' \\ \sqrt{G}\rho u^1 \\ \sqrt{G}\rho u^2 \\ \sqrt{G}\rho w \\ \sqrt{G}(\rho\theta)' \end{bmatrix}, \quad \mathbf{F}_1 = \begin{bmatrix} \sqrt{G}\rho u^1 \\ \sqrt{G}(\rho u^1 u^1 + p' G_h^{11}) \\ \sqrt{G}(\rho u^2 u^1 + p' G_h^{21}) \\ \sqrt{G}\rho w u^1 \\ \sqrt{G}\rho\theta u^1 \end{bmatrix} \quad \mathbf{F}_2 = \begin{bmatrix} \sqrt{G}\rho u^2 \\ \sqrt{G}(\rho u^1 u^2 + p' G_h^{12}) \\ \sqrt{G}(\rho u^2 u^2 + p' G_h^{22}) \\ \sqrt{G}\rho w u^2 \\ \sqrt{G}\rho\theta u^2 \end{bmatrix}$$

$$\mathbf{F}_3 = \begin{bmatrix} \sqrt{G}\rho\tilde{w} \\ \sqrt{G}\rho u^1 \tilde{w} + \sqrt{G}_h\sqrt{G}_v G_v^{13} p' \\ \sqrt{G}\rho u^2 \tilde{w} + \sqrt{G}_h\sqrt{G}_v G_v^{23} p' \\ \sqrt{G}\rho w\tilde{w} + \sqrt{G}_h p' \\ \sqrt{G}\rho\theta\tilde{w} \end{bmatrix}, \quad \mathbf{S}(\mathbf{U}) = \sqrt{G} \begin{bmatrix} 0 \\ \sqrt{G}_h\rho f(u^1 G^{21} - u^2 G^{11}) - M_\Gamma^1 \\ \sqrt{G}_h\rho f(u^1 G^{22} - u^2 G^{12}) - M_\Gamma^2 \\ -\rho' g \\ 0 \end{bmatrix}$$

- Note: M_Γ^1, M_Γ^2 are geometric terms associated with cubed-sphere topology, they have no vertical dependence for shallow atmosphere approximation.

Computational Domain (Horizontal)

Cubed-Sphere GLL Grid (Ne5Np4)
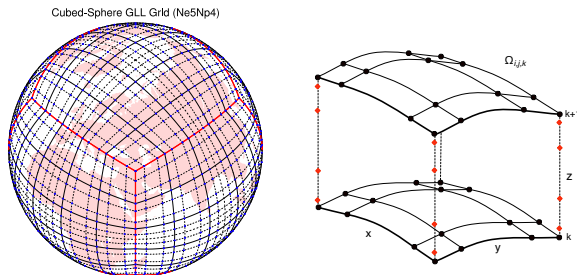
- Dimensional split approach: The computational domain $\mathscr{D}$ is decomposed into 2D + 1D. Independent DG discretization for horizontal (x^1, x^2) cubed-sphere surfaces, and vertical (ζ) direction.
- Cubed-sphere panel is tiled with non-overlapping $N_e \times N_e$ elements, each with $N_p \times N_p$ Gauss quadrature points. This is a standard setup in HOMME framework.
- Horizontal elements are stacked in the vertical direction, which forms the 3D grid system.

Computational Domain (Vertical)

HOMAM Vertical Grid Structure
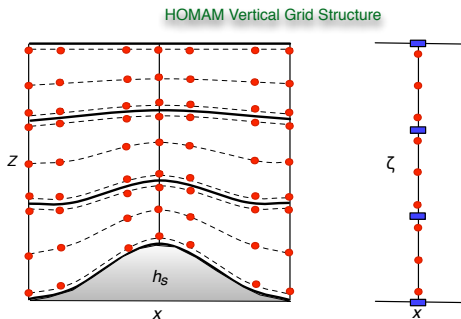
- The vertical grid line z or ζ is partitioned into V_{nel} 1D elements, each with N_g Gauss points. This is a major design change in HOMME/CAM framework.
- Currently Gauss-Legendre (GL) quadrature elements are used in the vertical, which define independent vertical levels with optimal accuracy.
- Total degrees-of-freedom (dof) is $6N_e^2 N_p^2 \times V_{nel} N_g$.
- Other possibilities: High-order FV discretization (WENO, Multi-Moment etc.)

Discontinuous Galerkin (DG) Methods in 2D

- DG Method is an ideal candidate for atmospheric model discretization, due to its inherent conservation proprty, geometric flexibility & parallel efficiency etc.

2D Scalar conservation law:

$$\frac{\partial U}{\partial t} + \nabla \cdot \mathbf{F}(U) = S(U), \quad \text{in} \quad (0, T) \times \mathscr{D}; \quad \forall (x, \zeta) \in \mathscr{D},$$

where $U = U(x, \zeta, t)$, $\nabla \equiv (\partial/\partial x, \partial/\partial \zeta)$, $\mathbf{F} = (F, G)$ is the flux function, and S is the source term.

Domain $D = \cup \Omega_{i,j}$

$\Omega_{i,j+1}$

Element
$\Omega_{i-1,j}$ $\Omega_{i,j}$ $\Omega_{i+1,j}$

$\Omega_{i,j-1}$
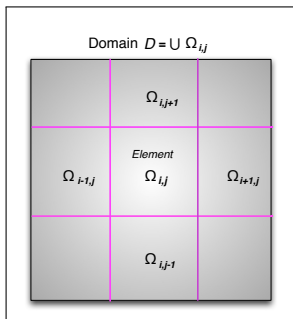
- The domain $\mathscr{D}$ is partitioned into non-overlapping elements Ω_{ij}
- Element edges are discontinuous
- Problem is locally solved on each element Ω_{ij}

DG-2D Spatial Discretization for an Element Ω_e in $\mathscr{D}$

- Approximate solution U_h belongs to a vector space $\mathscr{V}_h$ of polynomials $\mathscr{P}_N(\Omega_e)$.

- The Galerkin formulation: Multiplication of the basic equation by a *test function* $\varphi_h \in \mathscr{V}_h$ and integration over an element Ω_e with boundary Γ_e,

$$\int_{\Omega_e} \left[\frac{\partial U_h}{\partial t} + \nabla \cdot \mathbf{F}(U_h) - S(U_h) \right] \varphi_h d\Omega = 0$$

- Weak Galerkin formulation : Integration by parts (Green's theorem) yields:

$$\frac{\partial}{\partial t} \int_{\Omega_e} U_h \, \varphi_h \, d\Omega - \int_{\Omega_e} \mathbf{F}(U_h) \cdot \nabla \varphi_h \, d\Omega \quad + \int_{\Gamma_e} \mathbf{F}(U_h) \cdot \vec{n} \, \varphi_h \, d\Gamma = \int_{\Omega_e} S(U_h) \, \varphi_h d\Omega$$

- The analytic flux $\mathbf{F}(U_h) \cdot \vec{n}$ must be replaced by a numerical flux such as the local Lax-Friedrichs (Rusanov) Flux:

$$\mathbf{F}(U_h) \cdot \vec{n} = \frac{1}{2} \left[(\mathbf{F}(U_h^-) + \mathbf{F}(U_h^+)) \cdot \vec{n} - \alpha(U_h^+ - U_h^-) \right].$$

- For the Euler system, α is the upper bound on the absolute value of eigenvalues of the flux Jacobian $\mathbf{F}'(U)$.

$$\alpha \to \max\{|v^-| + c^-, |v^+| + c^+\}, c = \sqrt{\gamma R_d T}, \quad v^\pm = \mathbf{u}^\pm \cdot \vec{n}$$

$\alpha_{\max} = |u^i| + c\sqrt{G^{ii}}$ along x^i (horizontal) direction, and $\alpha_{\max} = |w| + c$ in the z-direction

DG Method: Nodal Spatial Discretization

- Every element Ω_e is mapped onto a unique reference element $[-1,1]^2$, with local coordinates $(\xi, \eta) \in [-1, 1]$.
- Construct a nodal basis set using a tensor-product of Lagrange polynomials $h_i(\xi)$, with roots at Gauss-Lobatto-Legendre (GLL) or Gauss-Legendre (GL) quadrature points $\{\xi_i\}$.
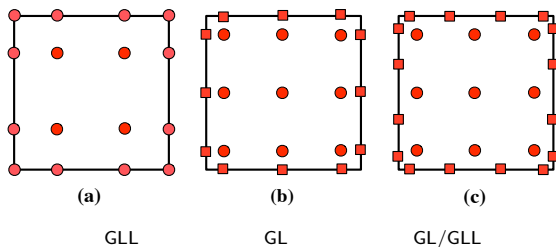- The nodal basis set is $\{h_i(\xi) * h_j(\eta)\}$ with

$$h_i(\xi)|_{GLL} = \frac{(\xi^2 - 1) P_N'(\xi)}{N(N+1) P_N(\xi_i)(\xi - \xi_i)} \quad \text{OR} \quad h_i(\xi)|_{GL} = \frac{P_{N+1}(\xi)}{P_{N+1}'(\xi_i)(\xi - \xi_i)}$$

- $P_N(\xi)$ is the Nth degree Legendre polynomial.
- The approximate solution and test functions are expressed in terms of basis function:

$$U_h(\xi, \eta) = \sum_{i=0}^{N} \sum_{j=0}^{N} U_{ij} h_i(\xi) h_j(\eta) \quad \text{for} \quad -1 \leq \xi, \eta \leq 1$$

- Final form for the discretization leads to a system of ODEs:

$$\frac{\partial \mathbf{U}}{\partial t} + \nabla \cdot \mathbf{F}(\mathbf{U}) = \mathbf{S}(\mathbf{U}) \quad \Rightarrow \quad \frac{d}{dt} \mathbf{U}_h(t) = \mathcal{L}(\mathbf{U}_h)$$

(a)	(b)	(c)
GLL	GL	GL/GLL

Pros & Cons

- The GL quadrature rule is exact for polynomials of degree up to $2N+1$, but the GLL quadrature rule is exact for polynomials of degree up to $2N-1$
- For a given *d.o.f*, the GL quadrature is more accurate as opposed to GLL. For relatively low-order approximations ($N \leq 4$), the GL quadrature is desirable.
- GL grid requires an interpolation of solution at the flux points ($\xi, \eta = \pm 1$), additional computational overhead.
- GLL results in inexact integration, but easy to implement and efficient. For high-oder ($N > 5$), GLL might be a better choice as the loss of accuracy is not significant.

DG-2D: Diffusion Process

Local Discontinuous Galerkin (LDG) method

- *Bassi and Rebay (JCP, 1997)* introduced a scheme for treating diffusion (viscuos flux) terms in DG discretization of the compressible Navier-Stokes equations.
- *Cockburn & Shu (1998)* generalized this approach known as the LDG method.

Consider the following advection-diffusion equation on an element Ω, with known (constant) diffusion coefficient ν.

$$\frac{\partial U}{\partial t} + \nabla \cdot \mathbf{F}(U) = \nu \nabla^2 U$$

- The key idea of LDG approach is the introduction of a local auxiliary variable $\mathbf{q} = \nu \nabla U$, and rewrite the above problem as a first-order system:

$$\mathbf{q} - \nu \nabla U = 0$$
$$\frac{\partial U}{\partial t} + \nabla \cdot \mathbf{F}(U) - \nabla \cdot \mathbf{q} = 0$$

- A robust approach, however, computationally expensive (uses wider stencil), and prohibitive for high-order diffusion (hyper-viscosity).
- More efficient approach based on Flux Reconstruction method may be desirable (Huynh, 2009).

The Diffusion Process: LDG method

- Multiplying by a vector test function $\Phi \in \mathcal{V}^d(\Omega)$, and integrating by parts

$$\int_\Omega \mathbf{q} \cdot \Phi \, d\Omega = \nu \left[\int_{\partial\Omega} U^* \Phi \cdot \vec{n} \, d\sigma - \int_\Omega U \nabla \cdot \Phi \, d\Omega \right]$$

- The weak formulation of advection-diffusion equation obtained using the test function ($\varphi \in \mathcal{V}(\Omega)$) and the Lax-Friedrichs flux $\hat{\mathbf{F}}$:

$$\begin{aligned}
\frac{\partial}{\partial t} \int_\Omega U \varphi \, d\Omega \quad &- \quad \int_\Omega \mathbf{F}(U) \cdot \nabla \varphi \, d\Omega + \int_{\partial\Omega} \hat{\mathbf{F}}(U) \cdot \vec{n} \, \varphi \, d\sigma \\
&+ \quad \int_\Omega \mathbf{q} \cdot \nabla \varphi \, d\Omega - \int_{\partial\Omega} \mathbf{q}^* \cdot \vec{n} \, \varphi \, d\sigma = 0,
\end{aligned}$$

- For the LDG method, numerical fluxes U^*, $\mathbf{q}^*$ are defined in terms of jump $[\cdot]$ and central $\{\cdot\}$ fluxes:

$$U^* = \{U\} + \beta \cdot [U], \quad \mathbf{q}^* = \{\mathbf{q}\} - \beta[\mathbf{q}] - \eta_k[U]$$

$$\{U\} = (U^+ + U^-)/2, \ [U] = (U^- - U^+)\vec{n}; \quad \{\mathbf{q}\} = (\mathbf{q}^+ + \mathbf{q}^-)/2, \ [\mathbf{q}] = (\mathbf{q}^- - \mathbf{q}^+) \cdot \vec{n}$$

- The constants $\beta = \vec{n}/2$ and $\eta_k = 0$ for the present application
- Robust approach, but computationally expensive (wider stencil), and prohibitive for hyper-viscosity

The Diffusion Process: Flux Reconstruction (FR) method

- Introduced by Huynh (2007, 2009). Unified DG, SD, SFV in a single framework.
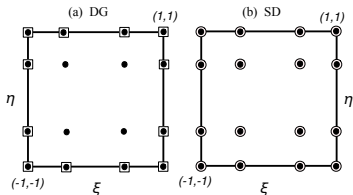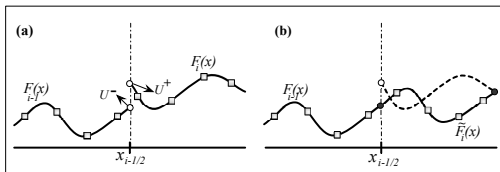
- Differential Form:

$$\frac{\partial U}{\partial t} + \nabla \cdot \mathbf{F}(U) = \mathbf{S}(U)$$

- Weak Galerkin Form (SE/DG methods):

$$\frac{\partial}{\partial t} \int_{I_{i,j}} U_h \, \varphi_h \, ds - \int_{I_{i,j}} \mathbf{F}(U_h) \cdot \nabla \varphi_h \, ds + \int_{\partial I_{i,j}} \mathbf{F}(U_h) \cdot \vec{n} \, \varphi_h \, d\Gamma = \int_{I_{i,j}} S_h \, \varphi_h \, ds$$

- Solve the differential form via spectral differencing (SD)
- At the element edges, continuity of fluxes are maintained by FR procedure

The Diffusion Process: Flux Reconstruction (FR) method

- For a simple conservation law, with a solution polynomial $U_i(x)$ of degree N

$$\frac{\partial U_i}{\partial t} + \frac{\partial F_i(x)}{\partial x} = 0 \quad \text{on} \quad I = [x_{i-1/2}, x_{i+1/2}]$$

- Reconstructed new flux,

$$\widetilde{F}_i(x) = F_i(x) + [\widehat{F}_{i-1/2} - F(x_{i-1/2})]\mathscr{G}_L(x) + [\widehat{F}_{i+1/2} - F(x_{i+1/2})]\mathscr{G}_R(x),$$

where $\mathscr{G}_L$ and $\mathscr{G}_R$ are the left and right correction functions (Radau polynomials) of degree $N+1$.

- DG or SD methods can be recovered by choosing suitable $\mathscr{G}_L, \mathscr{G}_R$ (Huynh, 2007):

$$\frac{\partial U_{i,k}}{\partial t} + \frac{\partial F_{i,k}}{\partial x} + [\widehat{F}_{i-1/2} - F(x_{i-1/2})]\mathscr{G}'_L(x_{i,k}) + [\widehat{F}_{i+1/2} - F(x_{i+1/2})]\mathscr{G}'_R(x_{i,k}) = 0,$$

For diffusion problem: $U_t = U_{xx}$

- Find the common value at the interface $\widehat{U}_{i+1/2} = (U^-_{j+1/2} + U^+_{j+1/2})/2$
- Find the common derivative the cell interface $x_{i+1/2}$, using FR procedure on elements I_i, I_{i+1} $[U_x]^{\text{com}}_{i+1/2} = ([U^R_i]_x + [U^L_{i+1}]_x)/2$. Find the second derivative U_{xx}.
- The process requires only 3-element wide stencil (I_{i-1}, I_i, I_{i+1}); i.e., one parallel communication.

The Diffusion Process: Flux Reconstruction (FR) method

- Evolution of vorticity for SW Test-case5 at Day 10 (*Williamson, 1992*)

Flow Over a Mountain: Relative Vorticity [Ne=18,Nv=6]
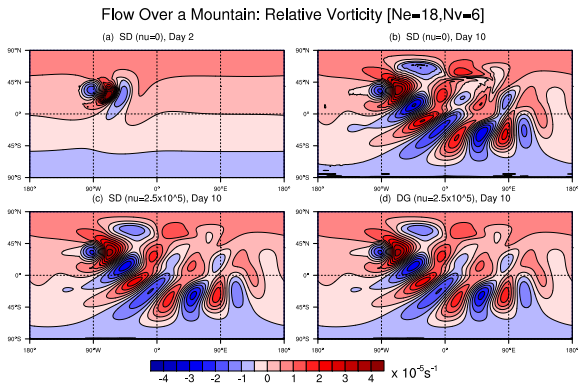
- Nodal viscous SW model, GLL grid with 6 points. FR can be implemented on existing DG/GLL stencils (quadrature-free implementation)
- About 20% more computational efficiency for viscous SW model [*Nair (MWR, 2015)*]
- Adopting FR philosophy $\Rightarrow$ "Goodbye" to Volume/Surface/Line integrals in DG formulation!

Time Stepping Challenges for the ODE system

For the resulting ODE systems:

$$\frac{dU_h}{dt} = L(U^h), \quad t \in (0, t_T)$$

where L is the DG spatial discretization operator.

Options & Challenges

- Explicit time integration efficient and easy to implement.
  Stringent CFL constraint $\Rightarrow$ tiny Δt, limited practical value.

$$\frac{C\Delta t}{\bar{h}} < \frac{1}{2N+1}$$

  1. $C = \max\{|u|+c, |w|+c\}$, $c = \sqrt{\gamma R_d T}$, dominated by fast moving acoustic waves and gravity wave.
  2. Minimum grid spacing $\bar{h} = \min\{\Delta x, \Delta z\}$, where $\Delta z \ll \Delta x$.
  3. P^N-DG, choose $N = \{2, 3, 4\}$, moderate order.
  4. Strong Stability-Preserving (SSP)-RK.

- Implicit time integration, unconditionally stable but generally expensive to solve. **Overall efficiency at a global scale is not known**.
- Semi-implicit time integration
  - Implicit solver for Linear part and explicit solver for nonlinear parts. Needs **efficient Helmholtz solver**.
  - HEVI: horizontal explicit and vertical implicit.

DG-NH Time Stepping-HEVI

For the resulting ODE system

$$\frac{dU_h}{dt} = L(U^h), \text{ with } \frac{C\Delta t}{\bar{h}} < \frac{1}{2N+1}$$

To overcome $\bar{h} = \min\{\Delta x, \Delta z\}$, treat the vertical time discretization (z-direction) in an implicit manner.

- **Benefit**: The effective Courant number is only limited by the minimum horizontal grid-spacing $\min\{\Delta x, \Delta y\}$.
- **Bonus**: The HOMME hydrostatic dynamical core relies on explicit time-stepping with excellent parallel scalability ($\mathcal{O}(10^5)$ processors). The 'HEVI' split approach might retain its parallel efficiency for NH equations too.
- Horizontal part and vertical part connected by **Strang-type** time splitting, permitting $\mathcal{O}(\Delta t^2)$ accuracy.
- **Remarks of HEVI**:
  - Particularly useful for 3D NH modeling ($\Delta z : \Delta x = 1 : 1000$).
  - Global NH models adopt the HEVI philosophy, NICAM[1], MPAS[2] etc.
  - Recent high-order FV-NH[3] models based on operator-split method.

---

[1]Satoh et al. 2008
[2]Skamarock et al. 2012
[3]Norman et al. (JCP, 2011), Ulrich et al. (MWR, 2012)

DG-NH Time Stepping with HEVI (Strang-type Split)

- Solve the ODE $d\mathbf{U}/dt = L(\mathbf{U})$ system, where $\mathbf{U} = (\sqrt{G}\rho', \sqrt{G}\rho u^1, \rho u^2, \sqrt{G}\rho w, \sqrt{G}(\rho\theta)')^T$.
- The spatial DG discretization corresponding to $L(\mathbf{U})$ is split into horizontal (H) and vertical (V) components, s.t. $L(\mathbf{U}) = L^H(\mathbf{U}) + L^V(\mathbf{U})$

$$\mathbf{U}_1 := \mathbf{U}_h(t), \qquad \frac{d}{dt}\mathbf{U}_1 = L^H(\mathbf{U}_1) \quad \text{in } (t, t+\Delta t/2]$$

$$\mathbf{U}_2 := \mathbf{U}_1(t+\Delta t/2), \qquad \frac{d}{dt}\mathbf{U}_2 = L^V(\mathbf{U}_2) \quad \text{in } (t, t+\Delta t],$$

$$\mathbf{U}_3 := \mathbf{U}_2(t+\Delta t), \qquad \frac{d}{dt}\mathbf{U}_3 = L^H(\mathbf{U}_3) \quad \text{in } (t+\Delta t/2, t+\Delta t],$$

and $\mathbf{U}_h(t+\Delta t) = \mathbf{U}_3(t+\Delta t)$.

- Possible options are is to perform "$H - V - H$" sequence of operations and "$V - H - V$" sequence.
- The vertical part may be solved implicitly with DIRK (Diagonally Implicit Runge-Kutta) [4].
- HEVI may be viewed as an IMEX Runge-Kutta (RK) method (Giraldo et al. 2009)
- For the implicit solver:
  - inner linear solver uses Jacobian-Free GMRES.
  - It usually takes 1 or 2 iterations for the outer Newton solver.

---

[4]Durran, 2010

HOMAM: 3D Advection DCMIP Benchmark Tests

- The transport equation in flux-from for a tracer variable q in 3D (x^1, x^2, z) coordinates can be written as

$$\frac{\partial \rho q}{\partial t} + \frac{1}{\sqrt{G_h}} \left[\frac{\partial}{\partial x^1}(\sqrt{G_h}\rho q u^1) + \frac{\partial}{\partial x^2}(\sqrt{G_h}\rho q u^2) + \frac{\partial}{\partial z}(\sqrt{G_h}\rho q w) \right] = 0$$

- In computational ζ-coordinate this reduces to

$$\frac{\partial \psi}{\partial t} + \frac{\partial(\psi u^1)}{\partial x^1} + \frac{\partial(\psi u^2)}{\partial x^2} = -\frac{\partial(\psi \tilde{w})}{\partial \zeta},$$

where the pseudo density $\psi = \sqrt{G}\rho q$, and $\sqrt{G} = \sqrt{G_h}\sqrt{G_v}$, is the "composite" Jacobian which combines the time-independent horizontal ($\sqrt{G_h}$) and the vertical ($\sqrt{G_v}$) metric terms.

- ρq is the conservative variable and $\tilde{w} = d\zeta/dt$ is the vertical velocity due to the coordinate transformation.

- DCMIP: https://earthsystemcog.org/projects/dcmip-2012/,
  Kent et al. (2014, QJRMS)

3D Advection Test: "Hadley-like" Meridional Circulation

- DCMIP-12: A deformational flow that mimics a "Hadley-like" meridional circulation.
- The wind fields are designed so that the flow reverses itself halfway through the simulation and returns the tracers to their initial position.
- The exact solution is known at the end of the run (1 day).
- HOMAM setup for $1°$ L60:
  $N_e = 30$, $N_p = 4$ (GLL);
  $V_{nel} = 15$; $N_g = 4$ (GL),
  $\Delta t = 60$ s, 1 day simulation.
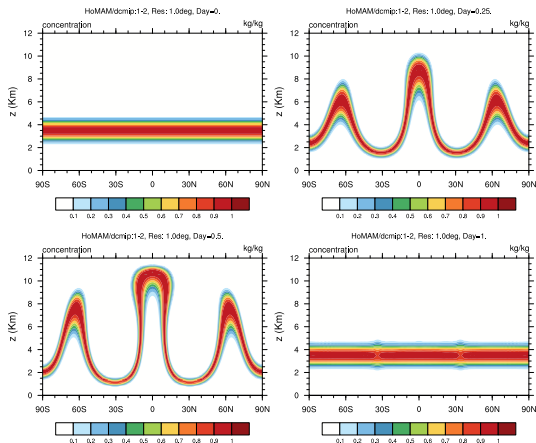
- HEVI, HEVE and Full (un-split) produce visually identical results.

3D Advection DCMIP-12 Test: Convergence
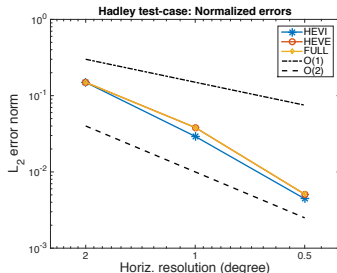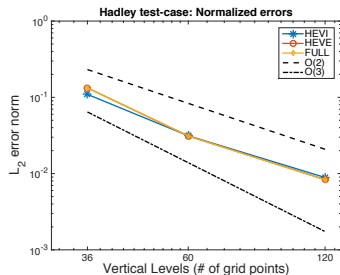
Convergence Rate: DCMIP, Kent et al. (2014), Hall et al (2015)

Errors/Models:	Mcore	CAM-FV	ENDGame	CAM-SE	HOMAM
ℓ_1	2.22	1.93	2.18	2.27	2.62
ℓ_2	1.94	1.84	1.83	2.12	2.43
ℓ_∞	1.64	1.66	1.14	1.68	2.16

Table: Average convergence rate for the normalized error norms for the Hadley test (DCMIP test 1-2) computed using resolutions $2°, 1°, 0.5°$ horizontal, and respectively with $30, 60, 120$ vertical levels.

- Temporal convergence is between 1st and 2nd-Order with the Hadley test.

3D Advection: Flow Over Rough Orography (DCMIP-13)
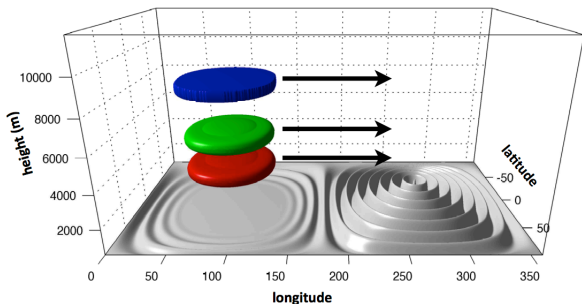
Figure: Schematic for DCMIP-13 test initial condition (*Figure courtesy: David Hall*)

- A series of steep concentric ring-shaped mountain ranges forms the terrain. The prescribed flow field is a constant solid-body rotation (Kent et al., 2014).
- The tracer field q is given by three thin vertically stacked cloud-like patches (non-smooth) which circumnavigate the globe and return to their initial positions after 12 days.

HOMAM: 3D Advection, Flow Over Rough Orography
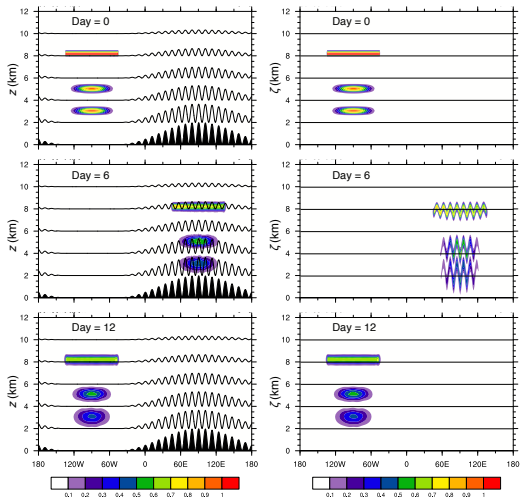
- HOMAM setup for $1°$ L120:
  $N_e = 30$, $N_p = 4$ (GLL);
  $V_{nel} = 30$; $N_g = 4$ (GL),
  $\Delta t = 6s$, 12 day simulation.

Error Norm	MCore $1°L120$	CAM-SE $1°L120$	HOMAM $1°L120$
ℓ_1	0.83	0.65	0.78
ℓ_2	0.55	0.27	0.50
ℓ_∞	0.73	0.75	0.76

[*Kent et. al. (2014); Hall et al. (2015)*]

- Vertical cross-sections along the equator for the tracer field q = q4 for the DCMIP test
- The results are simulated with HOMAM using the HEVE/HEVI scheme at a horizontal resolution of $1°$, 60 vertical levels, and $\Delta t = 12s$.

WENO-Based Monotonic (Bound Preserving) Limiter for DGM
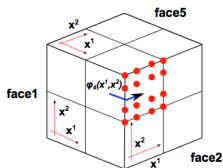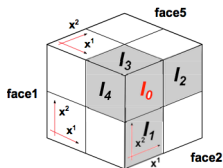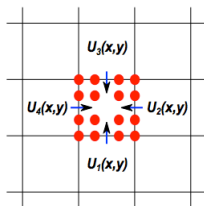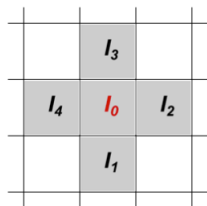
- Uses compact element stencils, ideal for cubed-sphere grids.
- Cell average $\overline{U}_{0,l}(\xi,\eta)$, $l = 1, 2 \ldots, 4$ is computed with

$$U_{0,l}(\xi,\eta) = \sum_{s=0}^{k} \sum_{m=0}^{k} U_l(\xi_s, \eta_m) h_s(\xi) h_m(\eta)$$

- Modify the coefficients $U_l(\xi_s, \eta_m)$ using WENO weights and local conservation as a constraint.
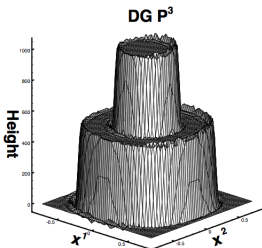- Apply local filter for positivity preservation

$$\tilde{U}_l(\xi,\eta) = \hat{\theta} U_l(\xi,\eta) + (1 - \hat{\theta})\overline{U}_{0,l}$$

$$\hat{\theta} = \max\left[|\frac{M - \overline{U}}{M_l - \overline{U}}|, |\frac{m^* - \overline{U}}{m_l^* - \overline{U}}|, 1\right]$$

- To be implemented in HOMAM

- *Guo, Nair & Zhong, (IJNMF, 2015)*

Advection on a cubed sphere

DG P³

DG P³+ WENO + BP
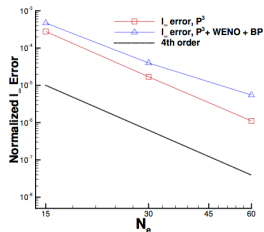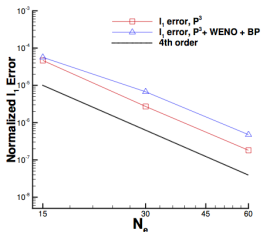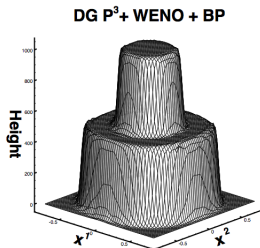
- WENO limiter controls internal oscillations, BP filter (optional) preserves positivity
- Convergence with solid-body rotation of a Gaussian field on the cubed-sphere. New limiter maintains high-order convergence

NH2D–DGP^2: Inertia-Gravity Wave Test (θ')

- The evolution of a potential temperature perturbation θ' (K) in a channel having periodic lateral and no-flux top/bottom boundary conditions. [*Skamarock & Klemp (1994)*]
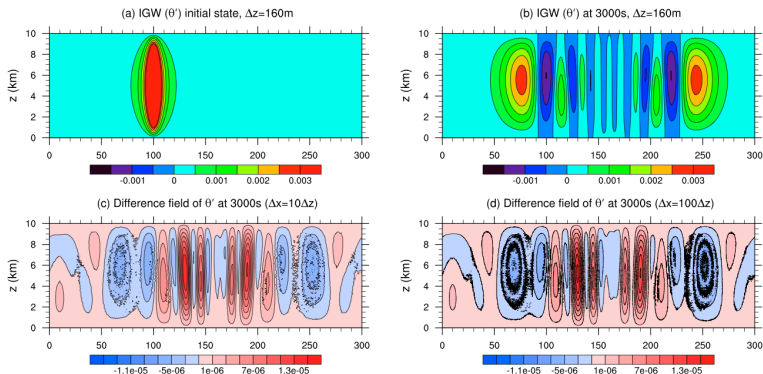
- Domain $[0, 300] \times [0, 10]$ km^2, T=3000 s. For $\Delta x/\Delta z = 10, 100$; $\Delta t = 0.14, 1.4$s, respectively. For the reference solution (explicit), $\Delta t = 0.014$s.
- Widely used for testing time-stepping methods in NH models, and $\Delta z \ll \Delta x$
- Ref: *Bao, Kloefkorn & Nair (MWR, 2015)*

Inertia Gravity Wave Convergence Study

HEVI-DG: Convergence with large aspect ratio $(1:100)$
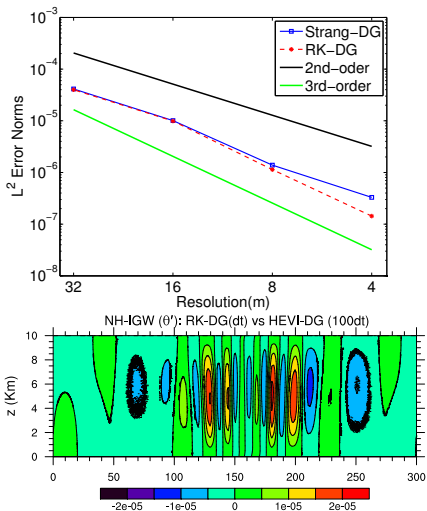
- $\Delta x = 100\Delta z$, i.e., 100 times larger Δt for HEVI-DG
- Difference field θ' is $O(10^-5)$.
- 2nd-order temporal convergence with a smooth test case.
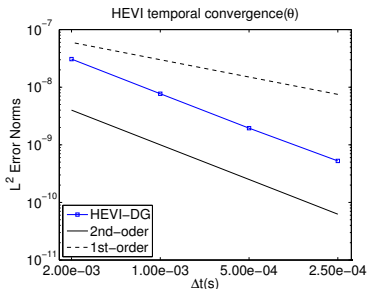
HOMAM: Nonhydrstatic Gravity Waves (DCMIP-31)

- NH Gravity Wave test (DCMIP-31) on a reduced planet ($X = 125$), θ' after 3600s
- $N_e = 25, N_p = 4, N_g = 4$ ($\Delta x \approx \Delta z \approx 1$ km), $\Delta t = 0.20$s
- The initial state is hydrostatically balanced and in gradient-wind balance. An overlaid potential temperature perturbation triggers the evolution of gravity waves.
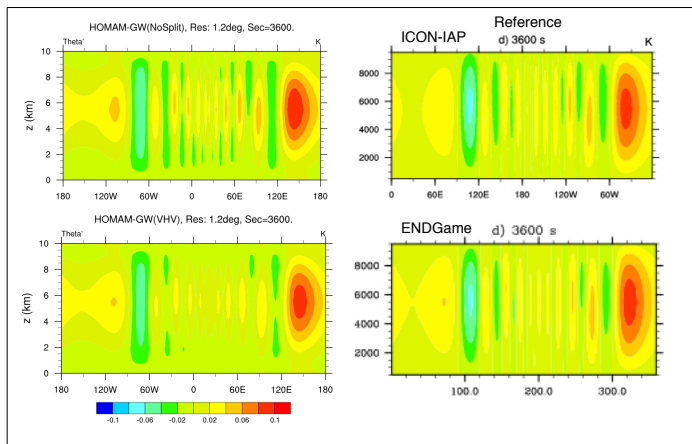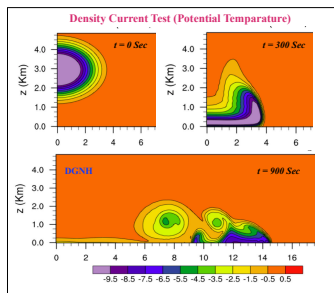
Nonhydrstatic Gravity Waves (DCMIP-31)
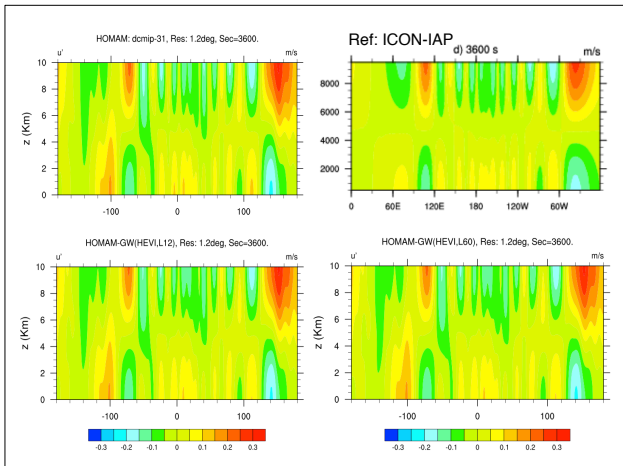
- NH Gravity Wave test (DCMIP-31) on a reduced planet ($X = 125$), U' after 3600s
- HEVI, HEVE produce identical results. HEVI is independent of the vertical CFL constraint

Straka Density Current [Straka et al. (1993)]

To validate Diffusion Process in HEVI-DG with LDG/FR

- Domain $[-26.5, 26.5] \times [0, 6.4] \, km^2$. $\theta = \overline{\theta} + \Delta\theta$;
- Initially, $\overline{\theta} = 300$K, $\Delta\theta = -15$K, $u = w = 0$.
- Simulated for 900 s, with diffusion ($\nu = 75.0 m^2/s$.) added to the momentum and the potential temperature equations.
- No-flux boundary conditions ($\mathbf{u} \cdot \mathbf{n} = 0$) are used for all boundaries
- Due to the symmetry, only half of the domain is shown

Straka Density Current: Diffusion LDG vs. FR

- Second-order diffusion with LDG and FR approach
- FR-Diffusion is found to be about 20% more efficient than that of LDG.

P2DG (100m, t=900s): Straka Current [θ']

P2-DG, (SD-Diff,dt=.05,100m): Density Current [θ']
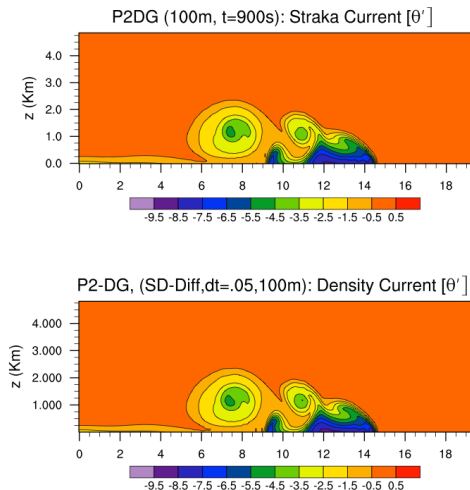
- Domain $[-26.5, 26.5] \times [0, 6.4]\, km^2$, simulated for $T = 900$s.
- $\Delta t = 0.05$s, $\Delta z = 100$m, $\Delta x = 100$m with P^2-DG and
- FR approach uses narrow stencil (nearest neighbor), results are comparable with that of LDG
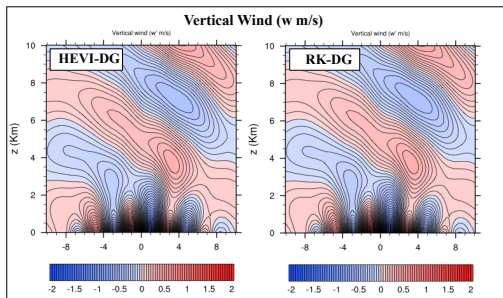
Schär Mountain (2D) Test [Schär et al. (2002)]

To validate Orographic influence on HEVI-DG splitting
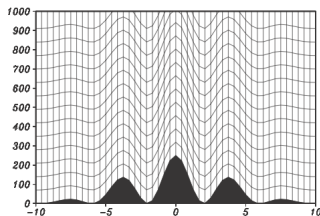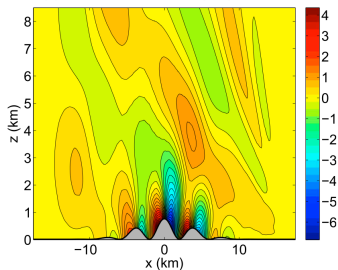

- The mountain profile

$$h(x) = h_0 \exp\left(-\frac{x^2}{a^2}\right) \cos^2\left(\frac{\pi x}{\lambda}\right)$$

- Domain $[-25, 25] \times [0, 10]$ km, simulated for $T = 10$h, and $h_0 = 250$m, $\lambda = 4$km, $a = 5$km, $u = 10$ m/s. (Non-reflecting BC)

- 50×25 elements, $\Delta t = 0.125$s, $\Delta z = 210$m, $\Delta x = 250$m with P^3-DG and RK-3 integrator.
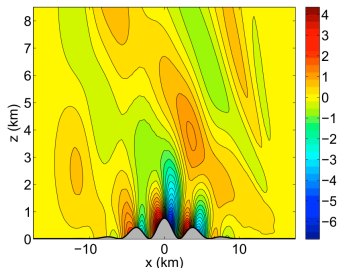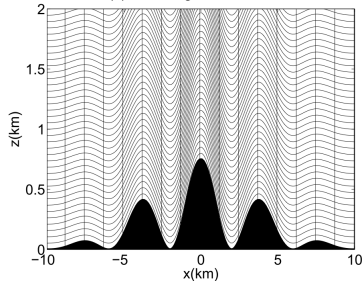
Schär Mountain Test-2

(e) HEVI: Vertical Wind w (m/s) at 1800s

(f) SSP−RK3: Vertical Wind w (m/s) at 1800s

(d) Schär High Mountain Grid

- w after 1800 s, with $\Delta t = 0.125 s$. P^3-DG (GL) discretization.
- Schär Mountain with higher elevation (max slope $\approx$ 55%)
- Virtually identical results with explicit RK3 and HEVI [*Bao, Kloefkorn & Nair (MWR, 2015)*]

Summary

- Early results with HOMAM Dycore (split and unsplit) are promising, and it performs well under benchmark test cases.
- Accuracy of the operator-split DG is acceptable.
- HEVI effectively relaxes the CFL constraint to the horizontal dynamics only, and permits significantly larger time step as opposed to the fully explicit method. Maintains $O(\Delta t^2)$ accuracy.
- New WENO-based limiter is effective and preserves high-order accuracy.
- The diffusion process via FR method is efficient, and accuracy is comparable to that of LDG, for SW and NH 2D models. Because of the compact stencil, FR is an efficient option for hyper-diffusion.

Future Work

- Complete all the DCMIP NH benchmarks for HOMAM (WIP)
- Improve the efficiency of HEVI time-stepping. For the horizontal part, employ multi-rate time integration scheme (subcycling).
- Adopt efficient preconditioner for the implicit solver in the vertical part. Test Hybrid-DG method for the implicit part. IMEX for HEVI etc.
- Test FR hyper-diffusion for HOMAM. Scalability study with large number of processors

Thank You!